Journal of Power Sources 195 (2010) 667–673

Contents lists available at ScienceDirect

Journal of Power Sources

journal homepage: www.elsevier.com/locate/jpowsour

MgO-templated nitrogen-containing carbons derived from different organic compounds for capacitor electrodes

Hidetaka Konno[a,*], Hiroaki Onishi[a], Noriko Yoshizawa[b], Kazuhisa Azumi[a]

[a] Laboratory of Advanced Materials Chemistry, Graduate School of Engineering, Hokkaido University, Sapporo 060-8628, Japan
[b] Energy Technology Institute, National Institute of Advanced Industrial Science and Technology, Tsukuba 305-8569, Japan

ARTICLE INFO

Article history:
Received 24 June 2009
Received in revised form 22 July 2009
Accepted 22 July 2009
Available online 29 July 2009

Keywords:
Electrochemical capacitor
Carbon containing nitrogen
Carbonization
MgO template method
Pseudo-capacitance

ABSTRACT

Carbons containing nitrogen (C–N composites) were derived from three commercial organic compounds, poly(vinylpyrrolidone) (PVP), polyacrylamide (PAA), and trimethylolmelamine (TMM) using the MgO template method. The C–N composites formed in nitrogen at 700–1000 °C had nitrogen content, W_N, of 3–23 mass% and the specific surface area by N_2 adsorption, S_{BET}, of 60–2000 $m^2\,g^{-1}$ without activation. Generally high nitrogen content of the starting compound led to larger W_N, but W_N was not proportional to the N/C mole ratio in the compounds. The value of S_{BET} strongly depended on the compound: S_{BET} (PVP) > S_{BET} (PAA) ≫ S_{BET} (TMM). There was a tendency for W_N to decrease with increasing S_{BET}. The capacitance measured in 1 mol dm^{-3} H_2SO_4 by cyclic voltammetry, C_M in $F\,g^{-1}$, suggested that both W_N and S_{BET} are influential in gaining large C_M. For the composites with W_N > 5 mass%, the capacitance normalized by S_{BET}, $C_A = C_M/S_{BET}$, was 0.17–0.65 $F\,m^{-2}$, which was larger than the electric double layer capacitance (0.05–0.15 $F\,m^{-2}$), indicating that the pseudo-capacitance contributes significantly to C_M. The value of C_A increased with increasing W_N, but a correlation between C_A and particular nitrogen species on the surface measured by XPS was obscure. It was suggested that the large C_A is not simply explained by redox reactions of the surface functional groups. The composite derived from PAA at 900 °C showed 234 $F\,g^{-1}$ at 2 mV s^{-1} and 181 $F\,g^{-1}$ at 100 mV s^{-1} with acceptable yield of the composite.

1. Introduction

The electric double layer capacitors (EDLCs) using organic electrolytes have high energy densities owing to high terminal voltages. However, taking costs, safety, and lifetime into consideration they are not necessarily the best suited to large scale installations for storage of the surplus power and the unsteady electricity produced by wind and others. Accordingly, electrochemical capacitors using aqueous electrolytes are not superfluous devices. For such devices, the activated carbons produced by sophisticated processes are possible to use, but the performance, especially energy density, is not quite satisfied for their prices. As promising electrode materials for aqueous electrolytes, transition metal oxides and nitrogen-doped carbons have been studied mainly aiming at high pseudo-capacitance. Increasing capacitance by nitrogen doping is often attributed to redox reactions of the nitrogen-containing functional groups [1], which is basically identical with the capacitance developed by transition metal oxides. For most of the nitrogen-doped carbons, however, the nitrogen content, W_N, is not sufficiently high to explain the gain in capacitance. There are additional rationales such as improving wetness of the pore walls by the formation of polar functional groups, increasing capacitance of the space-charge layer due to the increase in carrier concentration, and others [2]. At present, it is difficult to distinguish each contribution and reasonably explain the effect of nitrogen doping. Based on the above rationalization, reasonably high specific surface area, S_{BET}, should be favorable to increase the capacitance provided volumetric capacitance is not reduced excessively, though there are exceptions such as the carbons formed by the mica template method [3] and the carbonized melamine foam [4].

A simple procedure to form nitrogen-doped carbons is carbonization of nitrogen-containing organic compounds, mainly resins, but the subsequent activation processes to increase S_{BET} markedly reduce W_N [5–8]. Alternatively, activated carbons have been treated with nitrogen-containing compounds such as urea [8,9] and melamine [9]. However, the capacitance normalized by S_{BET}, C_A, of the material derived from brown coal [8], were 0.08–0.12 $F\,m^{-2}$, indicating that the capacitance is mainly attributed to the electric double layer. For the materials derived from wood-based activated carbons followed by melamine treatment, C_A reached 0.33 $F\,m^{-2}$ [9], suggesting the contribution of the pseudo-capacitance due to nitrogen. In contrast to the methods described above, both need activation processes, a method using silica templates successfully synthesized the carbonaceous

* Corresponding author. Tel.: +81 11 706 7114; fax: +81 11 706 7114.
E-mail address: ko@eng.hokudai.ac.jp (H. Konno).

0378-7753/$ – see front matter © 2009 Elsevier B.V. All rights reserved.
doi:10.1016/j.jpowsour.2009.07.039

materials which had S_{BET} = 807 m^2 g^{-1} and W_N = 7.2 mass% [10] and S_{BET} = 1330 m^2 g^{-1} and W_N = 10 mass% [11] without activation. The materials showed C_A = 0.25 F m^{-2} [10] and C_A = 0.16 F m^{-2} [11], but the methods of template preparation are not simple and the templates must be dissolved in hydrofluoric acid solutions [10,11].

Several years ago, the MgO template method was reported [12–17], which can form microporous and/or mesoporous carbons with high S_{BET} by pyrolysis of organic polymers, such as poly(vinyl alcohol) (PVA), poly(ethylene terephthalate) (PET), hydroxy propyl cellulose (HPC), and others. The process consists of the pyrolysis at 900 °C in an inert atmosphere followed by dissolution of template in a sulfuric or hydrochloric acid solution, and the activation process is not included. The pore formation mechanism is described elsewhere [12–16]: briefly, pitch-like materials formed by pyrolysis of polymer sink through MgO nano-particles and they coat the particles with thin carbonaceous layers, then by further carbonization the layers shrink to form porous carbons. This method is possible to start from a solution containing water-soluble polymers and magnesium salts [14–17]. The porous carbons formed by this method have been evaluated as electrode materials for EDLC [16,17]. So far, however, combinations of the polymers containing nitrogen and the MgO template are not reported.

In the present work, three commercial organic compounds of different nitrogen content were carbonized using the MgO template method to synthesize the carbons containing nitrogen (C–N composites), where mixed solutions of the compound and magnesium acetate were used as the starting materials. The objectives of the present work are (1) to survey the conditions to form the C–N composites with moderately high S_{BET} and large W_N, (2) to find the effect of S_{BET} and W_N on both C_M in F g^{-1} and C_A in F m^{-2}, and (3) to understand the role of doped nitrogen in the development of pseudo-capacitance.

2. Experimental

The organic compounds used were poly(vinylpyrrolidone) (PVP, Tokyo Chemical Industry), polyacrylamide (PAA, Aldrich), and trimethylolmelamine (TMM, S-260 supplied by courtesy of Nippon Carbide Industries). The PVP and PAA were reagent grade 50 mass% aqueous solutions and the average molecular mass was 10,000 for both. Based on the chemical structure, N/C mole ratio is 1/6 for PVP, 1/3 for PAA, and 1/1 for TMM, and the nominal nitrogen content is 12.6 mass% for PVP, 19.7 mass% for PAA, and 38.4 mass% for TMM. Thermal decomposition behavior of these compounds was examined by thermogravimetry (TG, SII TG/DTA6300) at 10 K min^{-1} in pure nitrogen. Magnesium acetate was used as a magnesium source, and hereafter the amount is expressed as a reduced value to MgO. A 10 mass% aqueous solution of PVP or PAA was prepared and set amounts of magnesium acetate were added. The TMM powder was dispersed in water and adequate amounts of ethanol were added to dissolve TMM with stirring, then set amounts of 50 mass% aqueous magnesium acetate solution were added. The mixing ratio of compound/MgO, in mass, was set to 3/7 or 5/5. It has been reported that a ratio of 3/7 provides the carbon materials of high specific surface area from PVA, PET and HPC [15]. The solutions were evaporated to dryness at 90 °C and pulverized with an agate mortar and pestle to obtain powder precursors.

The precursors were heated at 300 K h^{-1} to a set temperature in a range of 700–1000 °C and kept for 1 h at each temperature in a flow of pure nitrogen. The products were ground and dispersed into 1 mol dm^{-3} H_2SO_4 by ultrasonic stirring to dissolve MgO. Hereafter, formed C–N composites are referred to as PAA37-900 and so on, in the order corresponding to the starting compound, a mixing ratio, and a heat treatment temperature (HTT) in Celsius. The products were characterized by X-ray diffraction (XRD; Rigaku RINT2200, Cu Kα, 40 kV, 20 mA), nitrogen adsorption/desorption measurements at 77 K (BEL Belsorp-mini), elemental analysis, X-ray photoelectron spectroscopy (XPS; PHI ESCA-5800, monochromatic Al Kα, 300 W), and transmission electron microscopy (TEM; TOPCON EM002B, 120 kV).

The composites were fabricated to working electrodes by mixing with acetylene black and PTFE, 10 mass% each, and by pressing onto titanium mesh. The capacitance, C_M in F g^{-1}, was evaluated by integrating a cyclic voltammogram (CV) measured by a three electrode system, with Pt counter and SCE reference electrodes, in 1 mol dm^{-3} H_2SO_4. The potential range was −0.2 to +0.8 V vs. SCE, and the potential scan rate, r, was 2–100 mV s^{-1}. Galvanostatic time–potential curve measurements were carried out at 0.5 and 1 A g^{-1} in 1 mol dm^{-3} H_2SO_4 by the three electrode system described above. The value of C_M was calculated with respect to the total mass of composite (the active material).

3. Results and discussion

3.1. Characterization of raw materials and C–N composites

As TMM was not reagent grade, the chemical composition was determined by elemental analysis: C 33.2, H 5.3, N 44.3, and the balance of oxygen, all in mass%, the nitrogen content was larger than the nominal one.

The mass changes by TG for PVP, PAA, and TMM are shown in Fig. 1. As magnesium acetate decompose to MgO below 250 °C [14], conversion of these compounds to carbonaceous materials starts after the formation of MgO. The curves for PVP and PAA coincide with the thermal decomposition behavior by the static method (residence time 1 h) reported previously [18]. Thus, the carbon yield in a HTT range of 800–1000 °C is less than 5 mass% from PVP, around 20 mass% from PAA, and 30–35 mass% from TMM.

The XRD patterns for all the C–N composites showed broad 0 0 2 and faint 10 peaks of carbon, and no signal of MgO. A very weak Mg 1s peak was distinguished for PAA and TMM by XPS as shown in Fig. 2. For both, the intensity of Mg 1s peak by area was about 1% of C 1s peak. The binding energy, E_B, was corrected with E_B[C 1s] = 284.6 eV for the main component of carbon, though the energy shift was within the experimental error, 0.19–0.23 eV. The E_B[Mg 1s] is larger than 1304 eV for both PAA37-900 and TMM37-900, indicating that the component is MgO and not $Mg(OH)_2$ (E_B[Mg 1 s] < 1303 eV). The residue after elemental analysis was a few mass% for PAA37 and TMM37 composites, and none or trace for PVP37 composites. Thus, very small amounts of MgO parti-

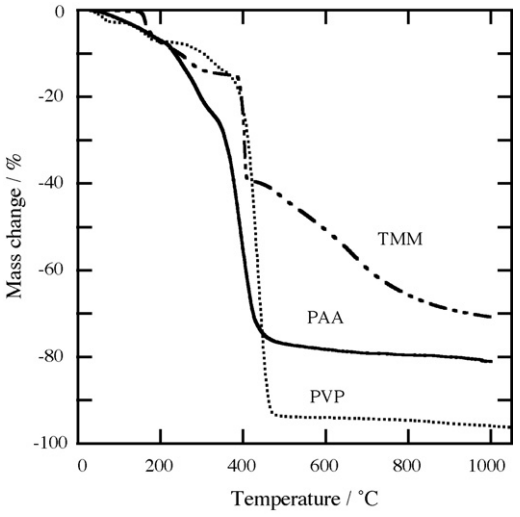

Fig. 1. Thermogravimetry of compounds in N_2 at 10 K min^{-1}.

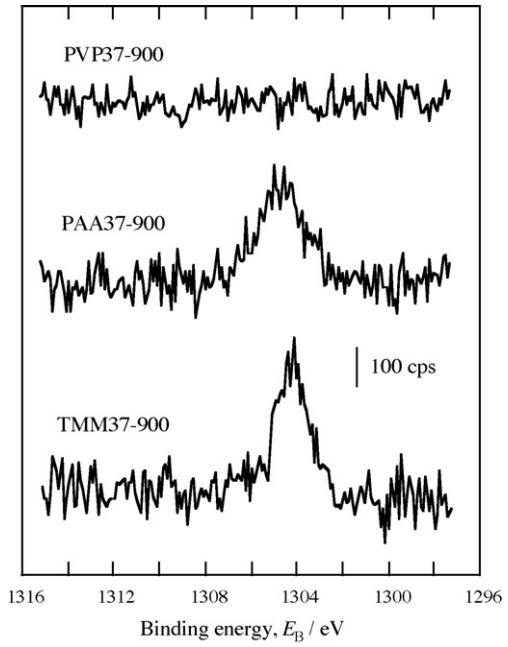

Fig. 2. XPS spectra of Mg 1s for the composites formed at 900 °C.

cles were covered perfectly with carbonaceous materials, which prohibited dissolution of MgO in the sulfuric acid solution. These results indicate that the remaining MgO particles may not affect to the capacitance. The N 1s spectra for the composites formed at 900 °C are shown in Fig. 3. Here the background lines were drawn by the empirical Shirley method [19] and the peak separation was carried out by assigning an identical peak profile (the same FWHM and Gaussian/Lorentzian mixing ratio) to each component in one spectrum. The number of peaks was changed from three to five and determined by the best convergence, that is, the number of peaks in Fig. 3 is not determined arbitrarily. The N components were numbered from lower E_B; peak I, E_B[N 1s] = 398.3–398.4 eV; peak II, E_B[N 1s] = 399.8–400.0 eV; peak III, E_B[N 1s] = 401.0–401.5 eV; and peak IV, E_B[N 1s] = 403.0–403.3 eV. An additional peak is observed at 405.2 eV for TMM37-900 but it was too weak to determine for PVP37-900 and PAA37-900. Each component is assigned as the following nitrogen species in carbon materials: peak I, pyridinic N (398.3 eV [20], 398.7 eV [21]); peak II, pyrrolic N (400.1 eV [20], 400.3 eV [21]); peak III, quaternary N (401.3 eV [20], 401.4 eV [21]), and peak IV, N-oxide (402–405 eV [21], 403.1 eV [22]). Notable points of Fig. 3 are (1) four common N components are present in the C–N composites irrespective of the starting compound but (2) a fraction of each N component in the three composites is different. It should be added here that it is senseless to use XPS for quantitative analysis of granular, and even porous, carbon materials: XPS data allow to calculate the mole ratios only when the surface is flat and composition of the surface layer is uniform in depth over a few times of the escape depth of photoelectrons. In the present case, compositional estimation is out of the question and only the ratio of different N components in one sample is significant information.

The nitrogen content, W_N, and the carbon content, W_C, are shown in Fig. 4. The hydrogen content was 1.7–2.8 mass% for all and decreased with increasing HTT. The data are the averages of two to four measurements. Generally W_C increases with increasing HTT, but there is no particular trend depending on the compound or the mixing ratio. The results indicate that the C–N composites formed at 700 °C and some formed at 800 °C are not carbonized enough. There is a plain tendency for W_N to decrease with increasing HTT and high nitrogen content of the starting compound leads

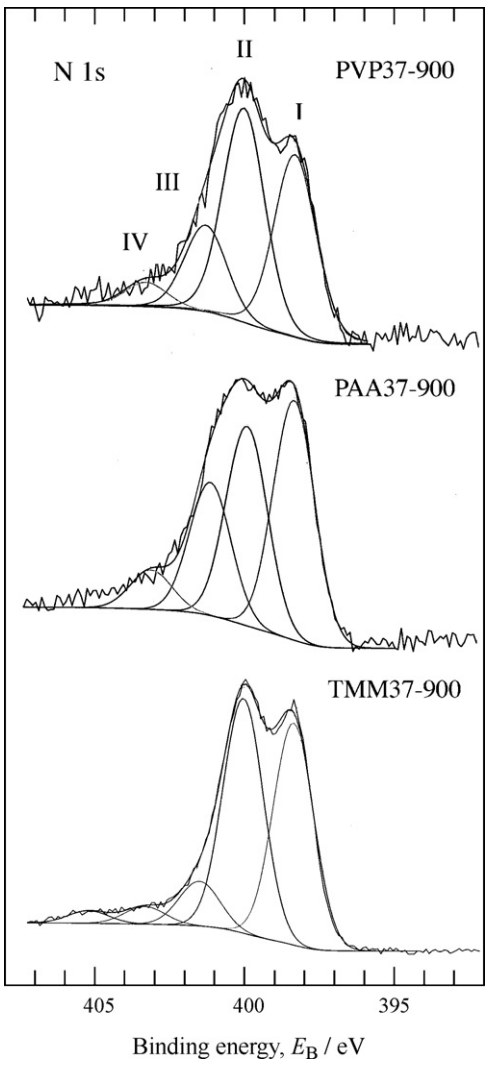

Fig. 3. XPS spectra of N 1s for the composites formed at 900 °C.

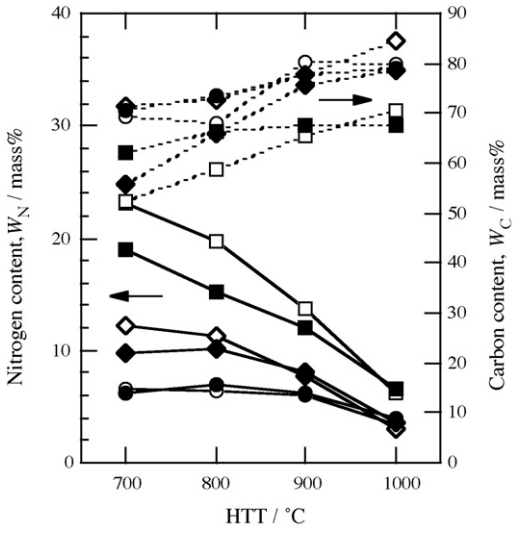

Fig. 4. Nitrogen and carbon content as a function of heat treatment temperature, HTT. Mixing ratios of compound/MgO are 3/7 (filled symbols) and 5/5 (open symbols): ● ○ PVP; ♦ ◇ PAA; ■ □ TMM.

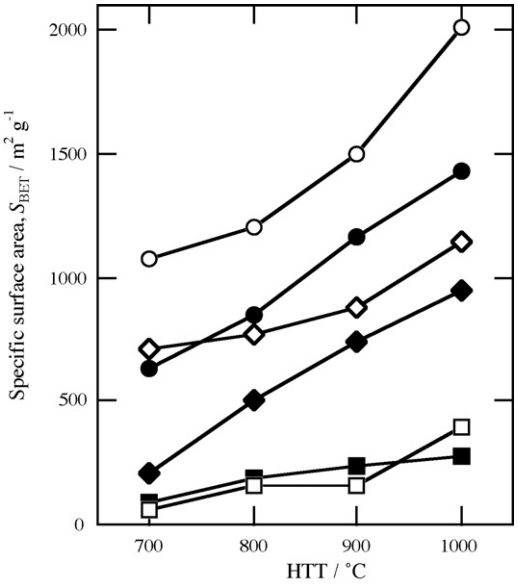

Fig. 5. The specific surface area, S_{BET}, as a function of HTT. Symbols are the same as Fig. 4.

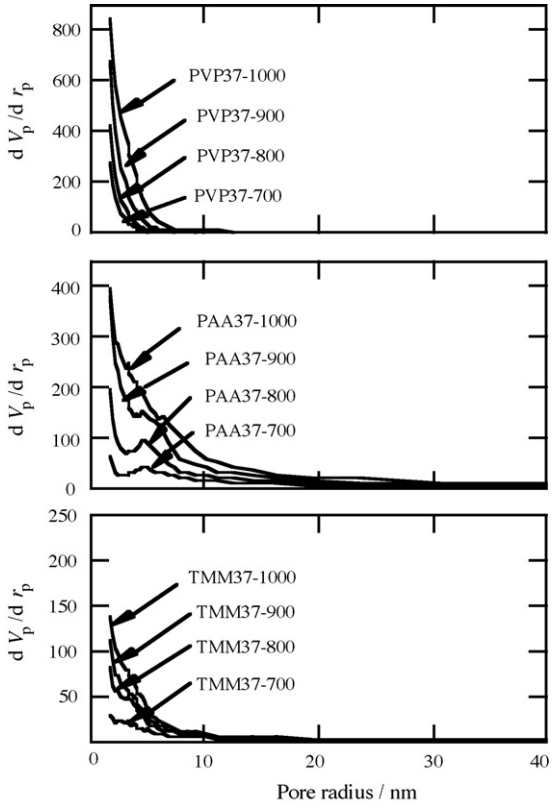

Fig. 6. Pore size distribution calculated from N_2 adsorption isotherms by the BJH method.

to larger W_N, though W_N is not proportional to the N/C mole ratio in the compounds. Further, in the case of relatively high yield compounds, PAA and TMM, W_N from the 5/5 precursors is larger than that from the 3/7 precursors. This may be due to the formation of thicker carbonaceous layers on MgO particles, leading to the lower loss of nitrogen. The balance of elemental analysis corresponds to the oxygen content but it should be noted here that adsorbed moisture may also be included. The apparent oxygen content is fairly high but a similar level of the balance (oxygen) is observed in the carbonized melamine foams in the same HTT range [4].

The value of S_{BET} increases with raising HTT as shown in Fig. 5, which is prominent for PVP and PAA. High S_{BET} is not attained with TMM. It has been reported that thermoplastic polymers must be used to prepare porous carbons by the MgO template method [13–15,17]. As melamine resins are thermosetting, TMM may also have similar property. As shown in Fig. 4, W_N decreases markedly by 1000 °C treatment. The results of Figs. 4 and 5 indicate that there is a tendency for W_N to decrease with increasing S_{BET}. This coincides with the reported trend that W_N decreases by activation [5–8]. The pore size distribution was calculated by the BJH method based on the nitrogen adsorption isotherms and shown in Fig. 6 for the composites derived from the 3/7 precursors. Pore size distributions for PVP37 and TMM37 composites are similar and the widths (two times of the pore radii in Fig. 6) are smaller than about 6 nm. In contrast the distributions for PAA37 composites are broad and a small peak is observed at around 4 nm in width. The diversity of S_{BET} and the pore size distribution depending on the compound is not simply understood, since the information about chemical and physical nature of the intermediate products formed by pyrolysis of the compounds is not available at present.

The TEM images of the C–N composites formed at 900 °C are shown in Fig. 7, in which typical pores (but not all) are indicated by circles. In PVP37-900 (Fig. 7(a)) circular transparent parts are mesopores of 4–6 nm in size, more or less, and many slit pores of 2–3 nm in width are observed in the upper part of the image. Large S_{BET} (Fig. 5) may be owing to these slit pores. In contrast, slit pores are not observed in PAA37-900 (Fig. 7(b)) and mesopores of 4–5 nm in size are scattered with bubble-like textures. In TMM37-900 (Fig. 7(c)) bubble-like textures similar to PAA37-900 and mesopores of about 5 nm in size are observed but generally micro-texture is dense and no slit pores. The MgO particles left in the composites were scarcely observed but one example in TMM37-900 is shown in Fig. 7(d). Dark spots similar to the sizes of mesopore in the left hand side are estimated to be MgO particles. Therefore, formation of mesopores is owing to MgO templates [11–16] and the evolution of slit pores is probably due to the thermal property of PVP, that is, about 95 mass% are released as gas by pyrolysis (Fig. 1). On the whole the features by TEM observation correspond to the pore size distributions in Fig. 6.

The C–N composites formed here are roughly characterized as follows: (1) the composites from PVP have low W_N but high S_{BET}, (2) the composites from PAA have moderately high W_N and S_{BET} but trade-off between W_N and S_{BET} is observed (Figs. 4 and 5), and (3) the composites from TMM have high W_N but low S_{BET}. In addition, a fraction of mesopores larger than 4 nm in size is higher in the composites from PAA than other two.

3.2. Capacitive performance of C–N composites

The CVs of 10th cycle in 1 mol dm^{-3} H_2SO_4 at $r = 2$ mV s^{-1} and $r = 20$–100 mV s^{-1} for PVP37-900, PAA37-900, and TMM37-900 are shown in Figs. 8 and 9, respectively. Although potential jumps at the lower and higher ends are steep at $r = 2$ mV s^{-1}, CVs are not neatly rectangular shape but broad bulges are distinguished in the middle part of CV for all electrodes (Fig. 8). These are often attributed to redox reactions of oxygen containing functional groups but they are too broad to determine what kinds of groups are responsible. The features of CV in Figs. 8 and 9 did not change after several tens to a hundred cycles in 1 mol dm^{-3} H_2SO_4. With increasing r the shape of CV is distorted but PAA37-900 is relatively unchanged at higher r. The capacitance calculated from CV is plotted against r in Fig. 10, where the composites of which C_M[100 mV s^{-1}] is less than 60% of C_M[2 mV s^{-1}] are omitted. For all the composites formed at 700 °C and the composites formed at 800 °C from TMM, C_M

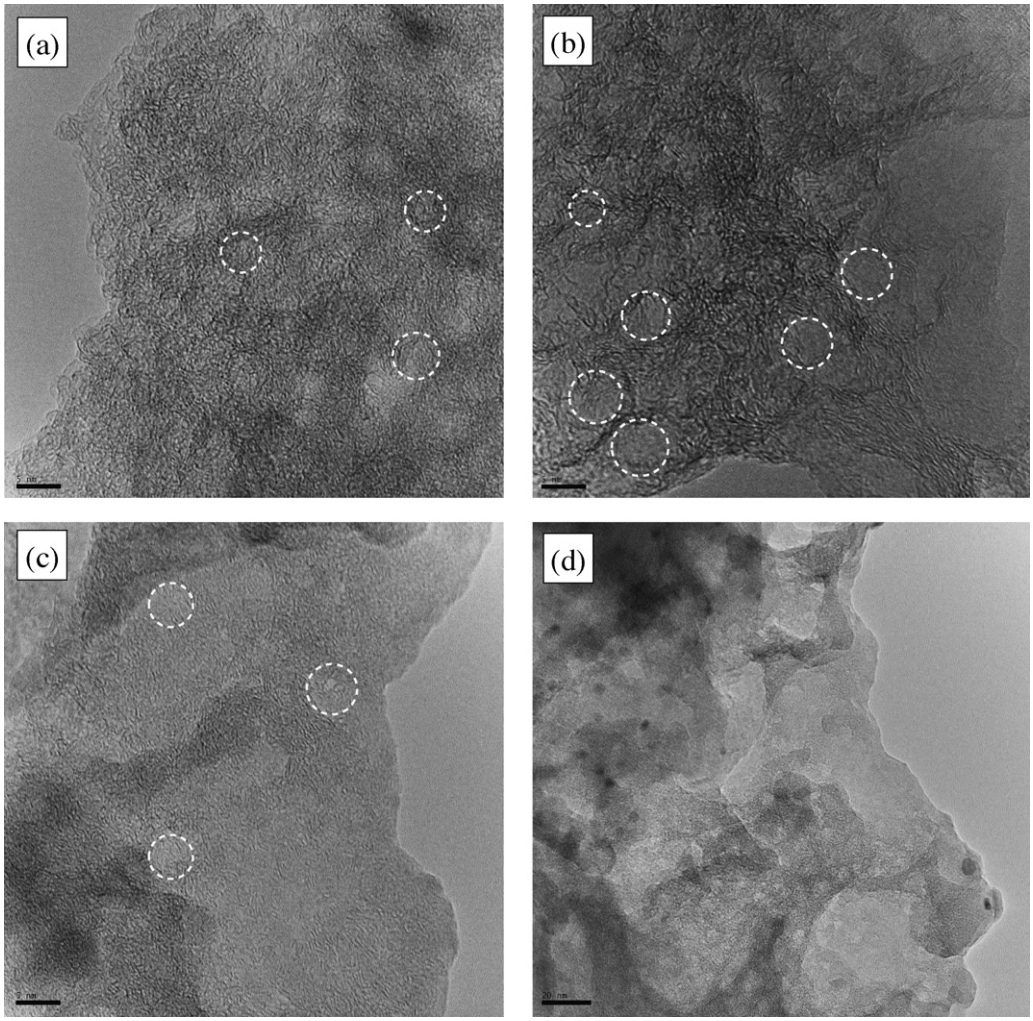

Fig. 7. TEM images of (a) PVP37-900, (b) PAA37-900, and (c) and (d) TMM37-900. Typical mesopores (not all) are indicated by circles. Scale bars in (a)–(c) are 5 nm and a bar in (d) is 20 nm.

drastically decreased with increasing r. It may be due to insufficient carbonization, leading to poor electric conductivity. Relatively high C_M and acceptable retention of C_M are achieved with PVP37-900, PVP37-1000, and PAA37-900: ratios of C_M[100 mV s^{-1}] to C_M[2 mV s^{-1}] are 164/243 = 0.675 for PVP37-900, 176/219 = 0.804 for PVP37-1000, and 181/234 = 0.774 for PAA37-900. As the carbon yield of PVP is rather low (Fig. 1), PAA37-900 will be the best in the present work. Galvanostatic time-potential curves in a potential range of −0.2 to +0.8 V vs. SCE for PAA37-900 are shown in Fig. 11. The potential changes are not neatly linear probably due to the pseudo-capacitance, but the charge/discharge time suggests the capacitance to be around 200 F g^{-1}.

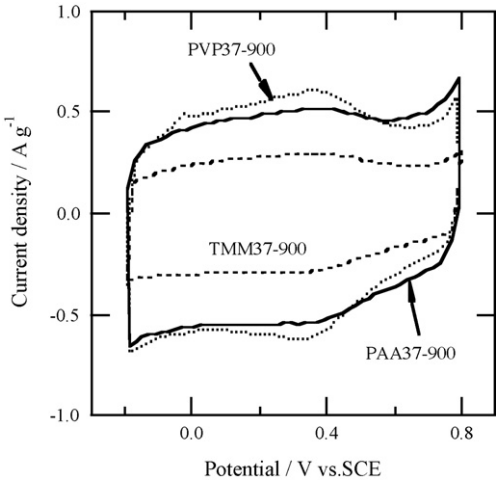

Fig. 8. Cyclic voltammograms at 2 mV s^{-1}.

The values of C_M and C_A at r = 2 mV s^{-1} for the composites formed at 800–1000 °C are summarized as a function of W_N in Fig. 12(a) and (b). The value of C_M at r = 2 mV s^{-1} for PVP55-1000 was unexpectedly low, 68 F g^{-1}, so that this was omitted. As the value of S_{BET} of this composite is exceptionally high (Fig. 5), there is a possibility that it was crushed and/or a large number of micropores were plugged during the preparation of electrode. Fig. 12(a) indicates that (1) large C_M of the composites from PVP is mainly due to higher S_{BET} (Fig. 5), (2) C_M of the composites from TMM does not increase appreciably with increasing W_N, which is probably attributed to lower S_{BET} (Fig. 5), and (3) for the composites from PAA, both W_N and S_{BET} contribute to gain large C_M (Figs. 4 and 5). Thus, C_M does not depend directly on W_N, while as shown in Fig. 12(b) C_A increases with increasing W_N en masse. The values of C_A are mostly larger than the electric double layer capacitance (0.05–0.15 F m^{-2}), excluding the composites with W_N < 5 mass%. It is evident that the pseudo-capacitance caused by nitrogen contributes significantly to the capacitance of composites. It should be added here that there

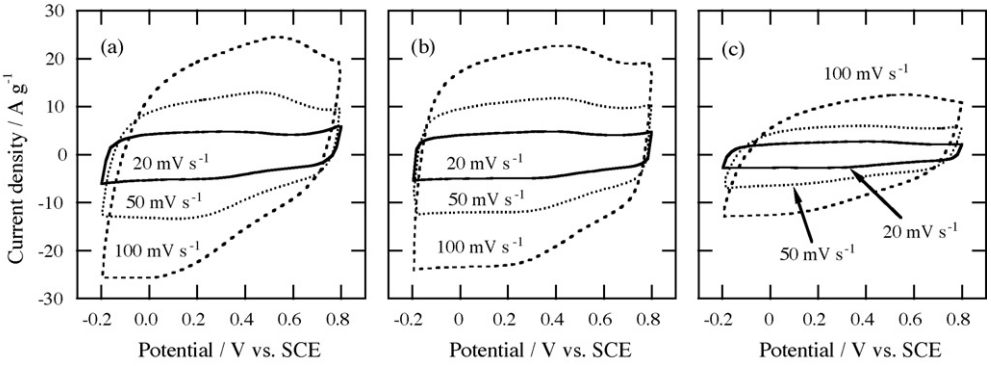

Fig. 9. Cyclic voltammograms at higher potential scan rates for (a) PVP37-900, (b) PAA37-900, and (c) TMM37-900.

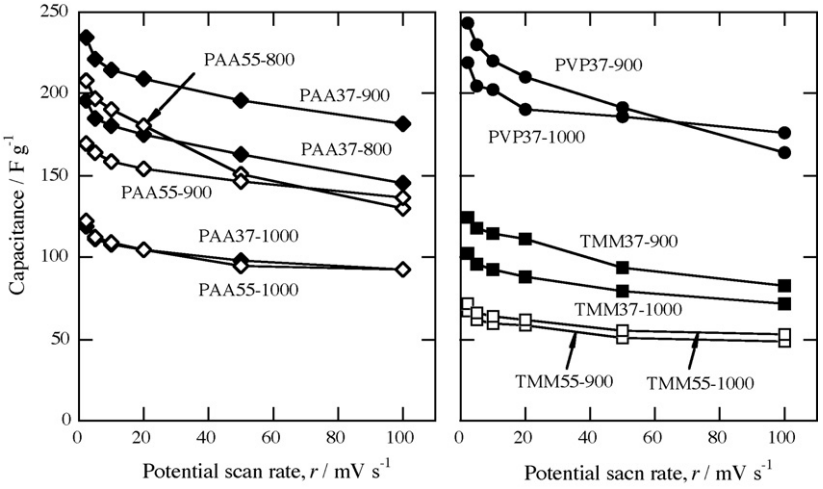

Fig. 10. The electrode capacitance, C_M in F g^{-1}, measured by cyclic voltammetry as a function of potential scan rate, r.

was no significant correlation between C_M and the oxygen content estimated from the balance of the elemental analysis. In Fig. 12, the effect of pore size distributions (Fig. 6) is not distinguished. However, there are a few points, which are difficult to understand. The values of W_N for the composites formed from TMM at 800 and 900 °C (Fig. 4) are comparable to those reported for the N-enriched carbon foams derived from melamine foam, but the values of C_M are much lower than those for the foams ($C_M > 200$ F g^{-1} [4]): the N-enriched carbon foams are reported to have very small S_{BET} by nitrogen adsorption. The pore size distribution of the composites from TMM is similar to that from PVP (Fig. 6). As TMM is a sort of monomer for melamine foam, it is difficult to explain why the performance (Figs. 8–10) is so different.

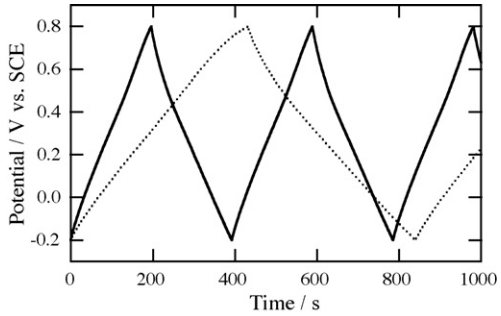

Fig. 11. Galvanostatic time–potential curves for PAA37-900 at 0.5 A g^{-1} (dotted line) and 1 A g^{-1} (solid line) in 1 mol dm^{-3} H_2SO_4.

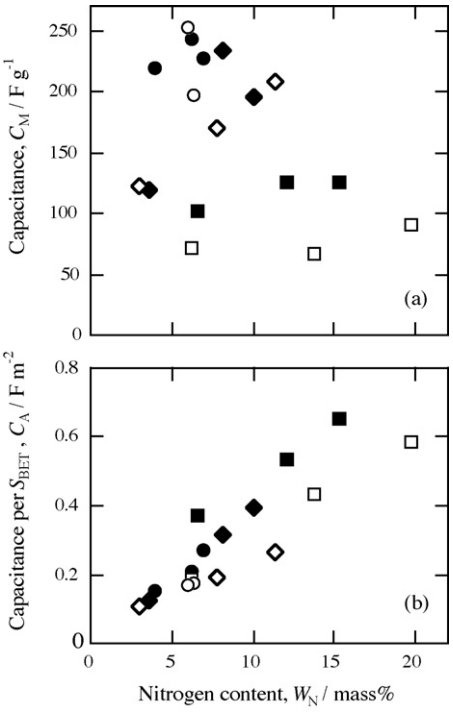

Fig. 12. (a) C_M and (b) C_A at 2 mV s^{-1} as a function of W_N. Symbols are the same as Fig. 4.

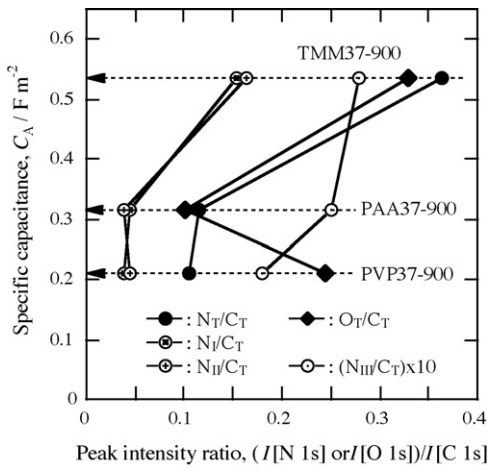

Fig. 13. Relationships between C_A at 2 mV s^{-1} and the surface compositions by XPS (see text for symbols).

To understand which type of nitrogen species mainly contributes to the pseudo-capacitance, the values of C_A for PVP37-900, PAA37-900, and TMM37-900 were compared with XPS data in Fig. 4. As described in Section 3.1, quantitative evaluation by XPS for these samples is dubious, so that only for rough survey C_A was plotted against the peak intensity ratios (by area) of each nitrogen component to the total carbon, N_I/C_T, N_{II}/C_T, and N_{III}/C_T, as shown in Fig. 13. The results, however, are obscure to argue that a particular nitrogen species is responsible to the pseudo-capacitance. Even, C_A is unlikely to be proportional to the total surface nitrogen, N_T/C_T. It may be possible to interpret a discrepancy between Fig. 12(b) and Fig. 13 in a way that the surface composition of nitrogen is different from that of the pore wall or that the main source of pseudo-capacitance is not the surface functional groups of nitrogen. However, still the case is not closed. Assuming the total site number of the surface to be 10^{19} atoms m^{-2} (this is a reasonable value for most of solid materials including carbon), the total electric charge accessible by one electron reaction is calculated to be 1.6 C m^{-2}. As the total capacitance becomes 1.6 F m^{-2} by 1 V of potential difference, the largest specific capacitance, 0.65 F m^{-2} (Fig. 12(b)), can be covered by about 40% of the total surface atoms (including those on the walls of accessible pores). The calculated results suggest, however, that the pseudo-capacitance observed for the composites cannot be attributed only to nitrogen, taking account of W_N (Fig. 4), even if the electric double layer capacitance is subtracted from the above value. Additionally, C_A is plotted against the intensity ratio of O 1s peak to C 1s peak, O_T/C_T, in Fig. 13, since the shape of CV in Fig. 8 suggests the contribution of oxygen containing functional groups. Unfortunately, the result is extremely deviated. As reliability of O 1s spectrum for this type of porous materials is low due to adsorption of moisture and other species containing oxygen, the peak separation of O 1s spectrum is insignificant.

At present it may be appropriate to conclude only that the pseudo-capacitance observed in the C–N composites is not explained by a single scheme, such as redox reactions [1,2].

4. Summary

Three commercial organic compounds, poly(vinylpyrrolidone) (PVP), polyacrylamide (PAA), and trimethylolmelamine (TMM) were carbonized at 700–1000 °C using the MgO template method starting from mixed solutions of the compound and magnesium acetate, and different types of C–N composites were formed. The results are summarized as follows:

(1) The nitrogen content, W_N, was 3–23 mass%. Generally high nitrogen content of the starting compound led to larger W_N, but W_N was not proportional to the N/C mole ratio in the compounds.
(2) The specific surface area by N_2 adsorption, S_{BET}, was 60–2000 m^2 g^{-1} and increased with increasing HTT. The value of S_{BET} strongly depended on the compound: S_{BET}(PVP) > S_{BET}(PAA) ≫ S_{BET}(TMM). There was a tendency for W_N to decrease with increasing S_{BET}.
(3) The capacitive behavior of the C–N composites formed in this work suggested that both W_N and S_{BET} are influential in gaining large capacitance, C_M in F g^{-1}.
(4) For the composites with W_N > 5 mass%, the capacitance normalized by S_{BET}, $C_A = C_M/S_{BET}$, was 0.17–0.65 F m^{-2}, which is larger than the electric double layer capacitance (0.05–0.15 F m^{-2}), indicating that the pseudo-capacitance contributes significantly to C_M.
(5) The value of C_A increased with increasing W_N, but a correlation between C_A and a particular nitrogen species on the surface measured by XPS was obscure. It was suggested that the large C_A is not simply explained by redox reactions of the surface functional groups.
(6) The PAA37-900 showed good performance as a capacitor electrode in 1 mol dm^{-3} H_2SO_4, in addition to acceptable yield of the composite. The ratio of C_M[100 mV s^{-1}] to C_M[2 mV s^{-1}] was 181 F g^{-1}/234 F g^{-1} = 0.774, indicating fair retention of capacitance.

Acknowledgements

The authors are grateful to Miss Mariko Ushiro and Mr. Keisuke Yoshizumi, Hokkaido University, for supplementary data. A part of the present work was supported by the Grant-in-Aid for Scientific Research (B) from JSPS (No. 18350102).

References

[1] D. Hulicova, J. Yamashita, Y. Soneda, H. Hatori, M. Kodama, Chem. Mater. 17 (2005) 241–247.
[2] Y. Yamada, O. Tanaike, S. Shiraishi, Tanso No. 215 (2004) 285–294.
[3] M. Kodama, J. Yamashita, Y. Soneda, H. Hatori, S. Nishimura, K. Kamegawa, Mater. Sci. Eng. B108 (2004) 156–161.
[4] M. Kodama, J. Yamashita, Y. Soneda, H. Hatori, K. Kamegawa, Carbon 45 (2007) 1105–1107.
[5] K. Jurewicz, K. Babe, A. Ziólkowski, H. Wachowska, M. Kozlowski, Fuel Process. Technol. 77–78 (2002) 191–198.
[6] G. Lota, B. Grzyb, H. Machnikowska, J. Machnikowski, E. Frackowiak, Chem. Phys. Lett. 404 (2005) 53–58.
[7] Y.J. Kim, Y. Abe, T. Yanagiura, K.C. Park, M. Shimizu, T. Iwazaki, S. Nakagawa, M. Endo, M.S. Dresselhaus, Carbon 45 (2007) 2116–2125.
[8] K. Jurewicz, R. Pietrzak, P. Nowicki, H. Wachowska, Electrochim. Acta 53 (2008) 5469–5475.
[9] M. Seredych, D. Huricova-Jurcakova, G.Q. Lu, T.J. Bandosz, Carbon 46 (2008) 1475–1488.
[10] E. Frackowiak, G. Lota, J. Machnikowski, C. Vix-Guterl, F. Béguin, Electrochim. Acta 51 (2006) 2209–2214.
[11] W. Li, D. Chen, Z. Li, Y. Shi, Y. Wan, J. Huang, J. Yang, D. Zhao, Z. Jiang, Electrochem. Commun. 9 (2007) 569–573.
[12] M. Inagaki, K. Kobayashi, F. Kojin, N. Tanaka, T. Morishita, B. Tryba, Carbon 42 (2004) 3153–3158.
[13] T. Morishita, R. Suzuki, T. Nishikawa, T. Tsumura, M. Inagaki, Tanso No. 219 (2005) 226–231.
[14] T. Morishita, R. Suzuki, T. Tsumura, H. Habazaki, M. Inagaki, Tanso No. 223 (2006) 220–226.
[15] T. Morishita, K. Ishihara, M. Kato, T. Tsumura, M. Inagaki, Tanso No. 226 (2007) 19–24.
[16] T. Morishita, K. Ishihara, M. Kato, M. Inagaki, Carbon 45 (2007) 209–211.
[17] T. Morishita, Y. Soneda, T. Tsumura, M. Inagaki, Carbon 44 (2006) 2360–2367.
[18] H. Konno, K. Fujita, H. Habazaki, M. Inagaki, Tanso No. 203 (2002) 113–116.
[19] D.A. Shirley, Phys. Rev. B5 (1972) 4709–4714.
[20] K. Stanczyk, R. Dziembaj, Z. Piwowarska, S. Witkowski, Carbon 33 (1995) 1383–1392.
[21] J.R. Pels, F. Kaptieijn, J.A. Moulijn, Q. Zhu, K.M. Thomas, Carbon 33 (1995) 1641–1653.
[22] S.R. Kelemen, M.L. Gorbaty, P.J. Kwiatek, Energy Fuels 8 (1994) 896–906.